Environmental Gradients Drive Shifts in Phytoplankton Community Structure

Jordan Winter[1], Annette Hynes[1], Chris Berthiaume[1], Kelsy Cain[1], E. Virginia Armbrust[1], François Ribalet[1*]

1 School of Oceanography, University of Washington, Seattle WA, USA

* ribalet@uw.edu

Abstract

Phytoplankton communities play an important role in marine food webs and biogeochemical cycles. Their size distribution and community structure are influenced by various environmental factors, including nutrient availability and temperature. This study investigates the dynamics of small phytoplankton (< 5 μm) across the eastern, southern, and northern boundaries of the North Pacific Subtropical Gyre (NPSG), using high-resolution, underway flow cytometry data collected during eight oceanographic cruises from 2016 to 2021. The cyanobacterium *Prochlorococcus* dominated within the gyre, with biomass ranging from 3.2 to 13.1 μgC L^{-1}, and its relative contribution to total phytoplankton biomass varied among cruises (31% to 81%, average 60 $\pm$ 16%). *Prochlorococcus* growth rates were significantly higher within the gyre (0.43 $\pm$ 0.18 per day) than outside the gyre (0.28 $\pm$ 0.16 per day) ($p < 0.001$). Northward, *Prochlorococcus* biomass and growth rates declined. Some variations in biomass and growth rates were observed southward and eastward, with biomass ranging from 3 to 10 μgC L^{-1} and growth rate ranging from 0.2 to 0.6 per day. Outside the NPSG, total phytoplankton biomass increased, with nanoeukaryotes becoming the predominant contributors (up to 71%, 9.1 $\pm$ 7.3 μgC L^{-1}). Picoeukaryote biomass also increased outside the gyre (up to 28 $\pm$ 12% of total biomass). Nutrient concentrations increased by nearly two orders of magnitude outside the NPSG, coinciding with the shift towards larger phytoplankton. The dominance of *Prochlorococcus* within the gyre emphasizes its adaptation to oligotrophic conditions, while the shift towards larger size classes outside the gyre likely reflects nutrient enrichment. The relatively low abundance of *Synechococcus* even in nutrient-rich regions suggest that that factors beyond nutrient availability, such as grazing, may influence its distribution. These findings have implications for understanding how phytoplankton communities will respond to future changes in oceanographic conditions, such as warming and altered nutrient regimes.

Introduction

Phytoplankton are the primary producers of oxygen and organic carbon in marine ecosystems, they form the base of oceanic food webs, and play an essential role in nutrient cycling [1]. Their cell size influences both spatial distributions and functional roles in marine biogeochemical cycles [2, 3] through modulation of biotic interactions, including grazing by zooplankton and competition with other phytoplankton, and abiotic interactions, including utilization of different concentrations and forms of nutrients. For example, picophytoplankton, which are less than 2 μm in diameter,

benefit from a high surface area-to-volume ratio that facilitates a more efficient nutrient uptake rate than that of larger cells [2]. This morphological trait is particularly advantageous in nutrient-poor waters, as exemplified by the predominance of the cyanobacterium *Prochlorococcus* (<0.6 μm) in the oligotrophic subtropical gyres, where it accounts for most of the primary production [2, 4, 5]. In contrast, larger phytoplankton, categorized as nano- and microphytoplankton (2-20 and 20-200 μm, respectively), are typically found in regions with higher nutrient availability [6]. Their larger cell size facilitates greater intracellular nutrient storage and a competitive advantage in nutrient-rich environments [2].

Several hypotheses have been proposed to explain the observed patterns in the size distribution of phytoplankton communities. The "rising tide" hypothesis suggests a relatively uniform response to nutrient enrichment, where an increase in nutrient supply leads to a proportional biomass increase across all phytoplankton sizes without altering the size structure of the community [7]. The "step addition" hypothesis posits that under conditions of high, stable nutrient supply, often seen in coastal regions, the biomass of larger phytoplankton increases due to their high nutrient uptake capacity, while the biomass of smaller size classes remains relatively constant [2]. The "enhanced microbial loop" hypothesis proposes that increases in nutrient supply trigger cascading effects throughout the food web, affecting not only phytoplankton but also bacteria, zooplankton and higher trophic levels. The resulting enhanced predation pressure, particularly on smaller cells that are preferentially consumed by grazers, can reshape the size structure of the phytoplankton community [8]. For example, the decline of *Prochlorococcus* with increasing nutrient supply, a pattern attributed to shared grazing pressure with heterotrophic bacteria [9], highlights the intricacies of these interactions. In this scenario, the increased nutrient supply supports not only the growth of larger phytoplankton but also heterotrophic bacteria. The expanding bacterial population, in turn, supports a larger population of grazers that feed on both bacteria and small phytoplankton like *Prochlorococcus*, leading to its decline despite the favorable nutrient conditions. Lastly, the "disturbance hypothesis" highlights how physical disturbances, such as mixing via mesoscale eddies, create a dynamic environment characterized by frequent fluctuations in nutrient availability. These conditions favor smaller, opportunistic phytoplankton, whose faster growth rates and resilience to disturbance-mediated dilution give them a competitive advantage in dynamically disturbed environments [10, 11]. These four hypotheses are not mutually exclusive as each offers a different perspective on the relationship between nutrient dynamics and phytoplankton community structure. Marine ecosystems are complex and the observed patterns are likely influenced by a combination of these hypotheses, varying in importance depending on the specific environmental conditions. Biotic and abiotic factors act concurrently, and sometimes antagonistically, to influence the size distribution of phytoplankton communities. This makes it challenging to fully understand the mechanisms driving patterns in phytoplankton size structure [12].

This study investigates how nutrient availability and temperature shape phytoplankton size distributions across the Northeast Pacific Ocean, encompassing the dynamic transition zone at the boundary of the North Pacific Subtropical Gyre (NPSG) as well as regions north, south and east of the gyre boundary. We collected continuous observations of the abundance and light scatter of small phytoplankton (< 5 μm) using the shipboard flow cytometer, SeaFlow, during eight oceanographic cruises that covered nearly 40,000 km across regions with different nutrient regimes, from the nutrient-poor NPSG to regions with higher nutrient availability [13]. The goal was to elucidate environmental drivers underlying the observed patterns in phytoplankton community structure and to evaluate the applicability of the various size distribution hypotheses in this dynamic region.

Table 1. Summary of cruises that transit from within to outside the NPSG.

cruise	direction	season	dates	duration (days)	travelled distance (km)
KOK1606	north	spring	2016-04-20 to 2016-05-04	15	3648
MGL1704	north	spring	2017-05-26 to 2017-06-13	19	4566
KM1712	north	summer	2017-07-31 to 2017-08-30	31	5504
KM1713	north	summer	2017-09-05 to 2017-09-26	22	3634
KM1906	north	spring	2019-04-10 to 2019-04-29	20	6263
KM1923	south	fall	2019-12-06 to 2019-12-16	11	3760
TN397	east, south	fall	2021-11-18 to 2021-12-15	28	7654
TN398	east	winter	2021-12-18 to 2021-12-30	13	4503

Materials and methods

Cruises

Eight cruises spanned from the NPSG to surrounding regions (Table 1), transiting to the north, east, and south of the gyre. These cruises ranged in duration from 11 to 31 days, spanning all seasons (spring: March to May, summer: June to August, fall: September to November, winter: December to February) from 2016 to 2021, and covered distances between 3634 km and 7654 km, totalling 39,532 km (Table 1). TN397 transited in multiple directions and was segmented into three distinct transects (TN397a, TN397b, and TN397c) for subsequent analysis. Each cruise was assigned a season based on the season in which the majority of its cruise days occurred.

Phytoplankton abundance and biomass

Phytoplankton abundance, size and biomass were measured using the underway flow cytometer SeaFlow, which continuously measures forward light scattering (457/50 nm bandpass filter), chlorophyll *a* fluorescence (692/40 nm bandpass filter), and phycoerythrin fluorescence (572/28 nm bandpass filter) of phytoplankton [14]. The instrument sampled directly from the underway seawater system collected from a depth of 3–8 m, depending on the ship. The incoming seawater was diverted into an overflowing bucket and from there pumped through a 100-μm stainless steel mesh filter to prevent clogging of the 200-μm sampling nozzle (Coulter ML05430) that forms the measurement stream. 1-μm yellow-green Fluoresbrite microspheres (Polysciences, Inc.) were continuously injected into the stream and served as standard beads.

Raw SeaFlow data were first processed as described in Ribalet et al. [15] to identify optimally positioned particles within the SeaFlow virtual core [14]. The resulting data were then analyzed using the R package popcycle 4.7.3 [15]. Four sets of gates were defined based on forward light scattering to classify 1-μm beads, the cyanobacteria (*Prochlorococcus* and *Synechococcus*) and small eukaryotes, as described in [16]. Small eukaryotes were further categorized into two populations based on their equivalent spherical cell diameter (see below for details): picoeukaryotes (<2 μm) and small nanoeukaryotes (2–5 μm).

The equivalent spherical diameter (ESD) of each cell was estimated from the flow cytometer forward light scattering signals by applying Mie light scatter theory based on three refractive indices (1.35, 1.38, 1.41) that cover the range applicable to marine phytoplankton [15]. As the scattering intensity can vary based on optical alignment, the choice of refractive index for *Prochlorococcus* and *Synechococcus* was chosen for each cruise based on the closest median ESD to 0.6 μm for *Prochlorococcus* near Station ALOHA [17]. Estimated cell diameters were converted to volume, assuming spherical particles, and then converted to carbon quotas using the equation $Q_{C,0} = 0.261$ x $V^{0.86}$,

where $Q_{C,0}$ is the carbon quota (pgC cell^{-1}) and V is the volume (μm^3) [18]. Mean cell abundances and mean carbon quotas were used to calculate carbon biomass concentrations for each population.

To better capture the spatial variability in biomass, we removed the day-night variability in biomass by applying a time series decomposition technique to the biomass data. This was achieved using a multiplicative decomposition model with a 24-hour moving window. This allowed us to isolate the trend in biomass and minimize the influence of short-term fluctuations caused by day-night cycles.

Data and code are available in Zenodo (DOI:10.5281/zenodo.14182976).

Cellular growth rate

Daily cellular phytoplankton growth rates were calculated from daytime increases in carbon quotas, based on the approach described in Hynes et al. [16]. To remove spatial variability and better capture daytime changes in carbon quotas, the hourly mean carbon quota (Q_C, pg C cell^{-1}) data were detrended using the same multiplicative decomposition model with a 24-hour moving window used for biomass data (see above). "Daytime" was defined as PAR values above 10 μmol photons m^{-2} s^{-1}. The daily cellular growth rate (r, h^{-1}) and the carbon quota at sunrise $Q_{C,0}$ were derived by fitting a transformed exponential growth function to the detrended carbon quota data:

$$\ln(Q_C) = r \times t + \ln(Q_{C,0}), \quad (1)$$

where t represents the number of hours since sunrise (h). To estimate cellular growth rate r, a given data series had to meet three conditions: 1) estimates were based on more than 30 observations per 3-minute file (i.e., cell abundance was $\geq 0.02 \times 10^6$ cells L^{-1}), 2) the daytime data spanned at least 6 hours, and 3) the p-values for the rate estimates were < 0.01 to be considered significant [16].

Environmental data

Salinity and temperature were measured underway using a Seabird Electronics SBE-21 thermosalinograph (Bellevue, WA, USA) and Photosynthetic Active Radiation (PAR) was measured with a Biospherical Instruments light sensor (San Diego, CA, USA). Dissolved inorganic nutrient (nitrate, nitrite, and phosphate) were obtained from unfiltered seawater, frozen, and analyzed on a SEAL Analytical Autoanalyzer (Mequon, WI, USA) while nitrate and nitrite concentrations below 5 μmol L^{-1} were analyzed with chemiluminescence [19]. Nutrient data were retrieved from Simons Collaborative Marine Atlas Project (Simons CMAP) [20].

Distance from the gyre boundary

The salinity front was used to estimate the gyre boundary and was defined as the maximum absolute derivative of salinity with respect to distance along each cruise track [9]. A spline was fitted to the salinity values to smooth high-frequency variations and improve accuracy before calculating the derivative. In cases where salinity changed multiple times along a cruise track, the salinity front closest to the average NPSG salinity of 35 PSU [9] was selected as the gyre boundary.

Data analysis

A Pearson correlation analysis was performed in R (version 3.6.2) between phytoplankton biomass, growth rates, and environmental factors to identify statistically

significant linear relationships (level of significance of 0.01) and quantify the strength of these associations. The correlation matrix included pairwise correlations between all phytoplankton groups (*Prochlorococcus*, *Synechococcus*, picoeukaryotes, and nanoeukaryotes), their biomass, growth rates, and the environmental variables (temperature, salinity, and concentrations of dissolved inorganic nitrogen and phosphorus). A one-way ANOVA test was conducted to validate the significance of the relationships identified in the Pearson correlation analysis. The environmental variables were used as factors and the phytoplankton biomass and growth rates were the response variables in the ANOVA. A Benjamini & Hochberg adjustment was applied to the p-values from the correlation analysis to control the false discovery rate at 0.01 [21]. The code is available in Zenodo (DOI:10.5281/zenodo.14182976).

Results

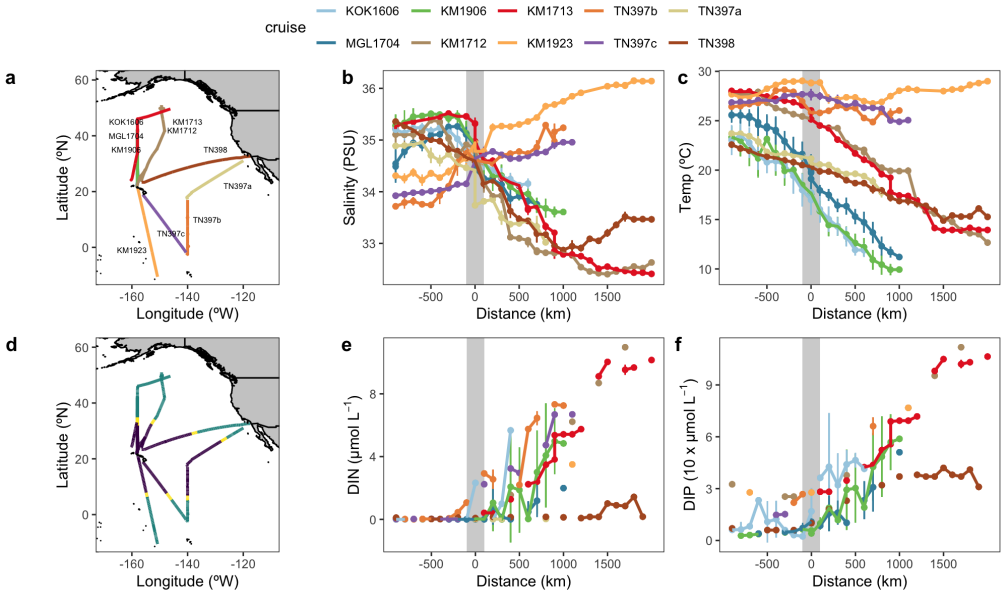

Fig 1. Environmental Gradients and Nutrient Distributions. (a) Cruise tracks, with each colored line representing a different cruise, with some cruises overlapping in certain regions (i.e., KOK1606, MGL1704, KM1906 and KM1712, KM1713 in the north). (b) Salinity (PSU) and (c) temperature (°C) along each cruise track, plotted as a function of distance (km) from the gyre boundary. (d) Each cruise was divided into three regions based on change in salinity (see Methods): the NPSG (purple), the gyre boundary (yellow), and the region outside the NPSG (teal). (e) Dissolved inorganic nitrogen (DIN) and (f) dissolved inorganic phosphorus (DIP) concentrations (μmol L^{-1}) along each cruise track. Negative distances indicate locations within the gyre, while positive distances represent locations outside the gyre. along each cruise track. Error bars represent standard deviations of the binned data over 100 km intervals. The gray shaded area highlights the gyre boundary.

The eight analyzed cruises (Table 1) sampled within both the North Pacific Subtropical Gyre (NPSG) and along transits to the north (KOK1606, KMG1704, KM1712, KM1713, KM1906), east (TN397a, TN398), or south (KM1923, TN397b and TN397c) of the NPSG (Fig 1a). For each cruise, distinct salinity fronts were detected at approximately 32 °N on the northern edge, between 5 and 7 °N on the southern edge,

and between 27 and 29 °N on the eastern edge (Fig 1b), which were used to define gyre boundaries [9]. Across the NPSG, sea surface temperatures ranged from 21 °C to 29 °C, with an average of 25.2 °C (Fig 1c). Within the northern and eastern regions of the NPSG, salinity and sea surface temperature generally decreased with increasing proximity to the gyre boundary. In the northern region (KOK1606, KMG1704, KM1712, KM1713, KM1906), salinity decreased from an average of 34.8 PSU to 34.1 PSU, and sea surface temperature decreased from an average of 26.3 °C to 20.6 °C. Similarly, in the eastern region (TN397a, TN398), salinity decreased from an average of 34.8 PSU to 34.1 PSU, while sea surface temperature decreased from 26.3 °C to 20.6 °C (Fig 1b, c). In contrast, within the southern region of the NPSG (KM1923, TN397b and TN397c), salinity increased from 33.5 PSU to 35.1 PSU with increasing proximity to the gyre boundary and were significantly lower than in other regions (one-sided t-test, $p < 0.001$), while sea surface temperatures remained relatively constant, averaging around 25.8 °C. Additionally, the average temperatures of the NPSG were lower during the winter and spring cruises (TN398, KOK1606, MGL1704, KM1906) (24.2 °C) than in summer and fall cruises (KM1712, KM1713, KM1923, TN397a,b,c and TN398) (25.4 °C) (one-sided t-test, $p < 0.001$).

Dissolved inorganic macronutrient concentrations increased by nearly two orders of magnitude along the northern and southern transects outside the NPSG. Dissolved inorganic nitrogen (DIN) concentrations increased from below 0.05 μmol L^{-1} within the gyre to almost 11 μmol L^{-1} outside and dissolved inorganic phosphate (DIP) increased from below 0.2 μmol L^{-1} within the gyre to 1.1 μmol L^{-1} at the northern-most station (Fig 1e, f). Similar increases in DIN and DIP were observed along the southern transects. In contrast, the two eastward cruises did not display similar increases in macronutrients, indicating that the gyre boundary does not always delineate the transition from oligotrophic to mesotrophic conditions and may involve a complex interplay of physical and biological processes.

Total biomass of the <5 μm phytoplankton was consistently higher outside the NPSG to the north than within the NSPG, averaging 19.7 ± 12.7 μgC L^{-1} outside and 11.1 ± 7.0 μgC L^{-1} within (Fig 2). For each phytoplankton group, changes in biomass were primarily driven by changes in cell abundance (Fig 2b), as cell size showed little variation inside and outside the gyre S1 Fig. Within the NPSG, the measured biomass was dominated by the cyanobacteria *Prochlorococcus*, with smaller proportional contributions by *Synechococcus*. With increasing distance outside the northern or southern gyre edges, the measured biomass became dominated by the small eukaryotic phytoplankton. In contrast, the relative proportion of different phytoplankton types remained relatively constant with distance from the eastern edge of the NPSG.

Prochlorococcus carbon biomass within the NPSG ranged from 3.2 to 13.1 μgC L^{-1} (Fig 2) and consistently dominated the total biomass of the small phytoplankton across all seasons and cruise directions. However, its relative contribution to the total biomass varied among cruises and ranged from 31% to 81%, with an average of 60% ± 16% (7.7 ± 2.0 μgC L^{-1}), with a notable 3-fold difference between the two southbound fall cruises (KM1923: 3.5 ± 1.5 μgC L^{-1}; TN397c: 9.7 ± 1.7 μgC L^{-1}). This variation in biomass (Fig 2a) was mirrored by changes in cell abundance (Fig 2b), which ranged from 2.9×10^8 to 0.9×10^5 cells L^{-1} within the NPSG. North of the gyre boundary, *Prochlorococcus* biomass declined sharply, dropping from the within-gyre average of 7.2 μg C L^{-1} to less than 1 μg C L^{-1} within 500 km. Southward, the decline in *Prochlorococcus* biomass was more gradual, with an initial decrease followed by a slight increase towards the southernmost points, except for TN397b where it continuously declined. East of the gyre, *Prochlorococcus* biomass remained relatively stable at ∼3 μg C L^{-1} before declining near the easternmost points, corresponding to the California coast (at 750 km and 1500 km east of the boundary for TN397a and TN398,

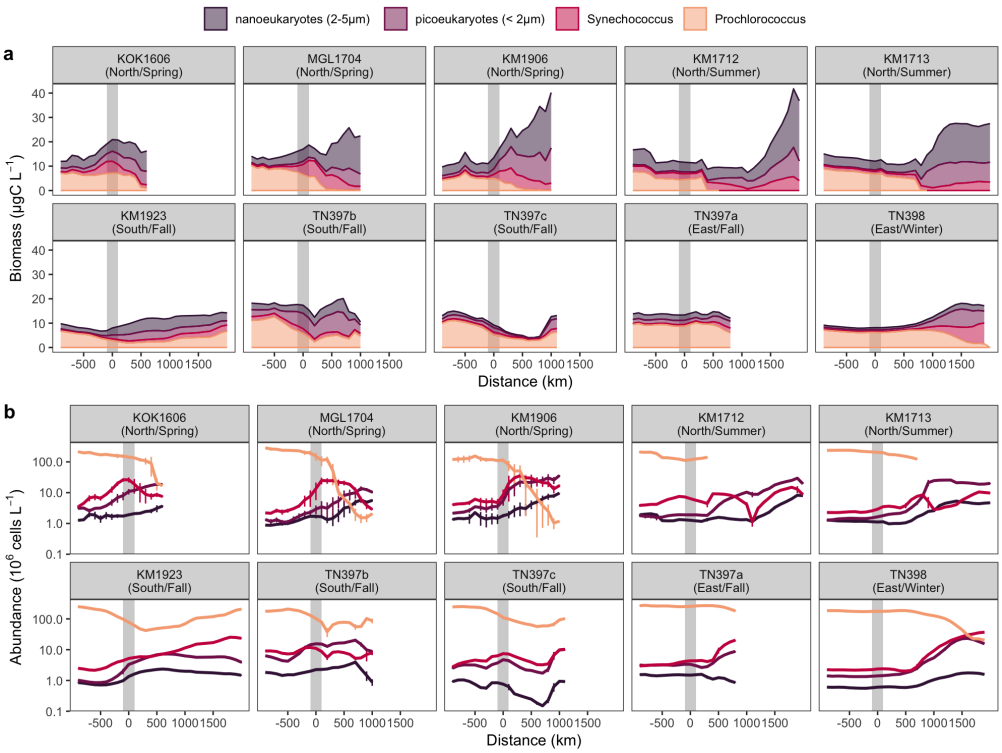

Fig 2. Phytoplankton Biomass and Cell Abundance Across Environmental Gradients a) Phytoplankton biomass (μg C L^{-1}) and b) cell abundance (10^6cells L^{-1}) relative to distance (km) from the gyre boundary (grey bar), with negative distances indicating locations within the gyre and positive distances representing locations outside the gyre. Colored lines represent the biomass of different phytoplankton groups: *Prochlorococcus* (orange), *Synechococcus* (red), picoeukaryotes (<2 μm, purple), nanoeukaryotes (2-5 μm, black). *Prochlorococcus* abundance drops below detection during KM1712 and KM1713 outside the gyre. Error bars represent standard deviations of the binned data over 100 km intervals.

respectively).

Synechococcus biomass was generally low within the NPSG (1.2 $\pm$ 0.9 μg C L^{-1}), consistent with the low cell abundance within the NPSG (4.9 $\times$ 10^6 $\pm$ 3.8 $\times$ 10^6 cells L^{-1}) (Fig 2b). Northward outside the gyre, *Synechococcus* abundance increased approximately 3 fold at the salinity front in spring (KOK1606, MGL1704 and KM1906), reaching 18 $\times$ 10^6 cells L^{-1} and contributing up to 47% (10.7 μgC L^{-1}) of the total phytoplankton biomass (Fig 2). This pattern was less pronounced to the east, with *Synechococcus* biomass and cell abundance remaining stable or slightly increasing with increasing distance from the gyre boundary. No such increase at the salinity front south of the gyre was observed.

Picoeukaryote biomass was low within the NPSG and increased outside the gyre, with the most substantial increase observed in the northern region (Fig 2a). In the north, biomass increased from an average of 1.0 $\pm$ 0.6 μg C L^{-1} inside the gyre to 6.4 $\pm$ 4.0 μg C L^{-1} outside, while in the eastern regions, the increase was more moderate (from 1.3 $\pm$ 0.5 μg C L^{-1} to 3.0 $\pm$ 2.3 μg C L^{-1}). This increase in biomass was accompanied by a corresponding rise in cell abundance, which increased from an average of 2.7 $\times$ 10^6 cells L^{-1} inside the gyre to 14.9 $\times$ 10^6 cells L^{-1} outside (Fig 2b)

Nanoeukaryotes also exhibited increased biomass outside the gyre, particularly in the

north, where they became the predominant contributors (up to 71%, 9.1 ± 7.3 μgC L^{-1}) and reached a biomass up to 27.4 μgC L^{-1}. This was mirrored by an increase in cell abundance from 1.3 × 10^6 cells mL^{-1} within the gyre to 3.4 × 10^6 cells mL^{-1} outside the gyre (Fig 2b). In contrast, nanoeukaryote biomass and abundance remained relatively stable in the southern region within the gyre 1.9 ± 0.6 μgC L^{-1} and 1.2 × 10^6 ± 0.4 × 10^6 cells mL^{-1}) and gradually increased towards the boundary in the eastern cruises.

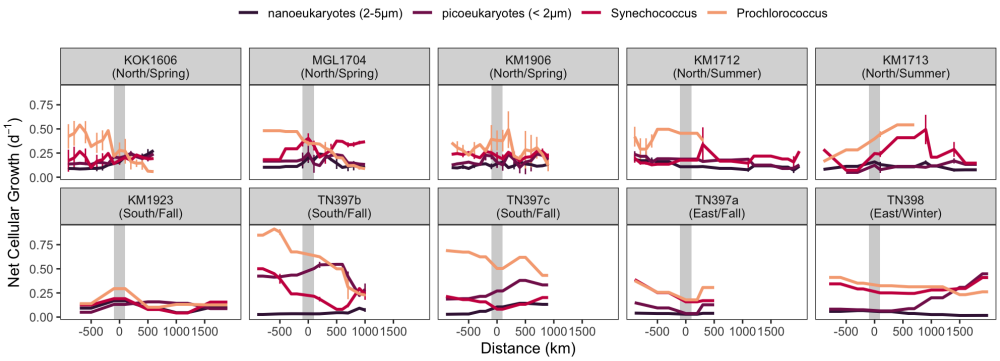

Fig 3. Phytoplankton Cellular Net Growth Rates Across Environmental Gradients Phytoplankton cellular growth rates (d^{-1}) relative to distance (km) from the gyre boundary (grey bar), with negative distances indicating locations within the gyre and positive distances representing locations outside the gyre. Colored lines represent the cellular growth rates of different phytoplankton groups: *Prochlorococcus* (orange), *Synechococcus* (red), picoeukaryotes (<2 μm, purple), nanoeukaryotes (2-5 μm, black). *Prochlorococcus* abundance drops below detection during KM1712 and KM1713 outside the gyre. Error bars represent standard deviations of the binned data over 100 km intervals. Note that error bars are shown when the ship spent more than 24 hours within a 100 km interval. DIN concentrations (μmol L^{-1}) are shown as black dots.

We used the change in per cell carbon quota over the daily cycle to estimate cellular net growth rates [16]. *Prochlorococcus* growth rates were generally higher within the gyre (0.43 ± 0.18 per day) compared to outside (0.28 ± 0.16 per day) (one-sided t-test, $p < 0.001$) (Fig 3). This pattern was particularly evident in two of the northern cruises (KOK1606 and MGL1704), where growth rates decreased outside the gyre as the cruises progressed northward into cooler waters, aligning with the observed decline in *Prochlorococcus* biomass (Fig 2a). However, *Prochlorococcus* growth rates was highly variable outside the gyre among other cruises, with some showing relatively constant net growth rates (TN398) or even increased net growth rates outside the gyre (KM1713). *Synechococcus* exhibited significantly lower overall net growth rates (0.24 ± 0.11 per day) than *Prochlorococcus* (0.36 ± 0.18 per day) (one-sided t-test, $p < 0.001$). *Synechococcus* growth rates were similar inside (0.26 ± 0.12 per day) and outside (0.23 ± 0.11 per day) the gyre (two-sided t-test, $p = 0.2$), with no clear trends related to cruise direction or location relative to the gyre boundary (Fig 3). Picoeukaryote net growth rates were not significantly different outside the gyre (0.18 ± 0.09 per day) compared to inside (0.20 ± 0.11 per day) (two-sided t-test, $p = 0.03$). Nanoeukaryotes displayed significantly lower net growth rates (0.11 ± 0.07 per day) than picoeukaryotes (0.19 ± 0.11 per day) (two-sided t-test, $p < 0.001$). Both picoeukaryote and nanoeukaryote growth rates were highly variable, with no clear pattern discernible in relation to the gyre boundary or cruise direction (Fig 3).

To further explore the factors influencing variations in growth rate and biomass, we examined the correlations between these phytoplankton measures with key

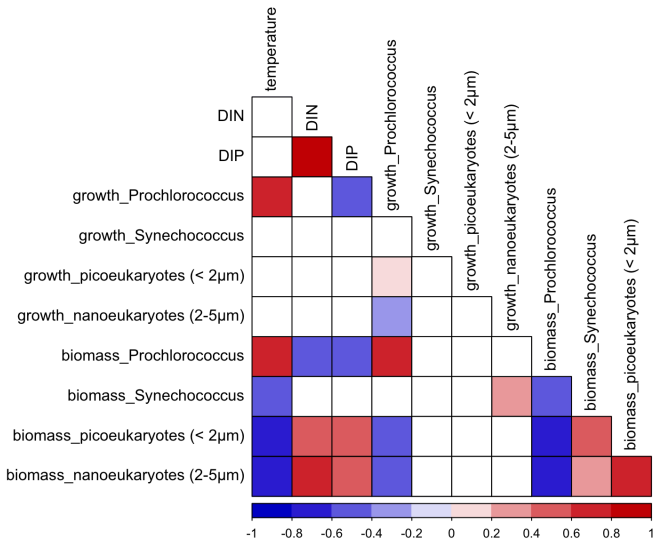

Fig 4. Nutrient-Phytoplankton Relationships. Correlation matrix between temperature, dissolved inorganic nitrogen (DIN) and dissolved inorganic phosphorus (DIP), cellular net growth rate of *Prochlorococcus*, *Synechococcus*, picoeukaryotes (<2 μm), nanoeukaryotes (2-5 μm), and their biomass. Correlations with a significance level < 0.01 are shown; positive correlations are in shades of red, negative correlations in blue, with color intensity indicating the value of the correlation coefficient (r).

environmental parameters, including temperature and nutrient concentrations. *Prochlorococcus* growth rate was positively correlated with temperature ($r = 0.60$, $p < 0.001$) and negatively correlated with DIP ($r = -0.39$, $p < 0.001$) (Fig 4). In contrast, the growth rates of *Synechococcus*, picoeukaryotes, and nanoeukaryotes showed no significant correlations with temperature or nutrient concentrations ($p > 0.06$ for temperature, and $p > 0.4$ for nutrients). A weak yet significant correlation was observed between the growth rates of picoeukaryotes and nanoeukaryotes with that of *Prochlorococcus* ($r = 0.1$ and -0.3, respectively, $p < 0.01$ for both). While the growth rates of *Synechococcus*, picoeukaryotes, and nanoeukaryotes appeared largely independent of the environmental factors examined, their biomass showed strong negative correlations with temperature ($r = -0.52$, -0.71 and -0.70, respectively, $p < 0.001$ for all). Furthermore, picoeukaryote and nanoeukaryote biomass showed positive correlations with both DIN ($r = 0.55$, $p < 0.001$ and $r = 0.66$, $p < 0.001$, respectively) and DIP ($r = 0.48$, $p < 0.001$ and $r = 0.56$, $p < 0.001$, respectively). Finally, biotic interactions likely further contributed to the observed patterns in biomass distribution. *Prochlorococcus* biomass were negatively correlated with *Synechococcus*, picoeukaryote and nanoeukaryote biomass ($r = -0.48$, -0.67, and -0.74, respectively, $p < 0.001$ for all), and picoeukaryote biomass was positively correlated with nanoeukaryote biomass ($r = 0.73$, $p < 0.001$).

Discussion

Our results demonstrate that the boundary of the NPSG is a critical region where dramatic shifts in phytoplankton community structure and size distribution occur. These shifts appear to be driven by a complex interplay of factors, including nutrient availability and temperature. The dominance of *Prochlorococcus* within the gyre across different seasons and cruise directions, highlights its remarkable adaptability to the oligotrophic conditions characteristic of this region. Its small size, high surface area-to-volume ratio, and efficient nutrient uptake mechanisms confer a competitive advantage in nutrient-poor waters, supporting the long-standing evidence of its significance in such environments [2, 4, 5]. However, the observed variability in *Prochlorococcus* biomass within the gyre suggest that factors beyond nutrient limitation influence its abundance. Temperature, in particular, emerged as a strong positive correlate of *Prochlorococcus* growth (r = 0.60) and biomass (r = 0.67)(Fig 4), suggesting its potential sensitivity to thermal regimes within the gyre. This variability contrasts with the more stable patterns observed at Station ALOHA [5, 16, 22], highlighting the dynamic and heterogeneous nature of the gyre environment, with a 10°C change in temperature and a 2 PSU variation in salinity observed across the gyre [1, 23].

The contrasting patterns observed in *Prochlorococcus* biomass and growth rates between northern and southern cruises underscore the influence of temperature on its distribution. The decline in biomass and growth rates in northward cruises, coinciding with decreasing temperatures, suggests a temperature-dependent limitation on its physiology, directly linking its physiological activity with population dynamics [24, 25]. This sensitivity to lower temperature, coupled with potential negative biotic interactions such as shared grazing pressure with heterotrophic bacteria [9] and shared viral lysis with *Synechococcus* [26], may contribute to the observed decline of *Prochlorococcus* populations in the northern regions, in agreement with ecosystem model predictions [12]. In contrast, the relatively stable biomass and growth rates observed in the warmer waters of the southern cruises, highlight *Prochlorococcus*' preference for higher temperatures. This further supports the growing body of evidence that temperature plays a crucial role in shaping the distribution and activity of *Prochlorococcus* in the ocean [24, 25, 27]. The favorable growth temperatures in the south and east of the gyre likely facilitate the persistence of *Prochlorococcus* populations [27]. Additionally, the advection of nutrients from the equatorial Pacific [28] and potential iron limitation [29] in these regions may prevent larger phytoplankton from outcompeting *Prochlorococcus* [30].

The substantial increase in total phytoplankton biomass and the shift towards larger size classes, particularly nanoeukaryotes, outside the gyre reflect a classic response to nutrient enrichment. This pattern aligns with the "step addition" hypothesis, which predicts an increase in the biomass of larger phytoplankton in response to greater nutrient supply [2].The ability of larger cells to store nutrients and capitalize on resource pulses likely contributes to their success in these more eutrophic regions. The positive correlations between nanoeukaryote biomass and both DIN and DIP (r = 0.61 and r = 0.38, respectively) support the notion that nutrient availability drives their growth. The dominance of nanoeukaryotes outside the NPSG, especially in northern cruises, emphasizes their ecological significance in these nutrient-rich environments [31]. However, nutrient enrichment did not uniformly increase biomass across all size classes as predicted by the "rising tide" hypothesis [7]. While the positive correlation between picoeukaryote and nanoeukaryote biomass (r = 0.69) suggests a degree of co-occurrence or shared environmental preferences for these two groups, *Prochlorococcus* biomass declined substantially outside the gyre. The negative correlations between *Prochlorococcus* biomass and both picoeukaryote and nanoeukaryote biomass (r = -0.70 and r = -0.67, respectively) hint at resource partitioning among these size classes or

potential competitive interactions. For instance, the decline of *Prochlorococcus* populations at the northern boundary of the NPSG has been attributed to increased grazing pressure and viral infections [12, 26, 32]. These nuances highlight the complex interplay between biotic and abiotic factors in shaping community structure.

While nanoeukaryotes thrive in these nutrient-rich conditions, smaller phytoplankton groups like picoeukaryotes and *Synechococcus*, exhibit more complex responses to nutrient enrichment, potentially due to limitations in nutrient competition and increased grazing pressure. Picoeukaryotes, for instance, may face limitations in nutrient competition due to their smaller size and lower nutrient storage capacity compared to nanoeukaryotes. Furthermore, the increase of nanoeukaryotes may also lead to an increase in "shared predators" that preferentially feed on smaller phytoplankton, keeping picoeukaryotes in check despite the increased nutrient availability, consistent with the "enhanced microbial loop" hypothesis [8]. *Synechococcus* presents an intriguing case. Its biomass and growth rates remain relatively low throughout the study area, even in nutrient-rich regions, suggesting that it is outcompeted by other phytoplankton or limited by grazing pressure. The only noticeable increase in *Synechococcus* biomass occurred near the salinity front, particularly to the north and east, suggesting a direct response to elevated nutrient levels outside the gyre. This localized increase could also be attributed to a shift in the grazing pressure. The abundance of carnivorous predators could be higher at the gyre boundary [33], which may reduce the grazing pressure on *Synechococcus*. Finally, the "disturbance hypothesis" highlights how physical disturbances, like those created at the boundary of the NPSG, create a dynamic environment characterized by frequent fluctuations in nutrient availability. These conditions may favor smaller, opportunistic phytoplankton like *Synechococcus*, whose faster growth rates and resilience to disturbance-mediated dilution give them a competitive advantage in dynamically disturbed environments. The combined effects of reduced grazing pressure and nutrient variability might explain the increased *Synechococcus* biomass at the boundary of the NPSG.

Conclusions

This study highlights the complex interplay of biotic and abiotic factors that shapes phytoplankton communities at the boundary of the NPSG. Our findings underscore the importance of nutrient availability, temperature, and biotic interactions in driving shifts in phytoplankton community structure and size distribution. The dominance of *Prochlorococcus* within the gyre emphasizes its adaptation to oligotrophic conditions, while the shift towards larger size classes outside the gyre reflects the influence of nutrient enrichment. However, the variability in *Prochlorococcus* biomass within the gyre and the complex responses of picoeukaryotes and *Synechococcus* to nutrient enrichment suggest that factors beyond simple resource availability contribute to the observed patterns. Future research should investigate the role of biotic interactions, such as grazing and viral lysis, in shaping community structure across the NPSG boundary.

Supporting information

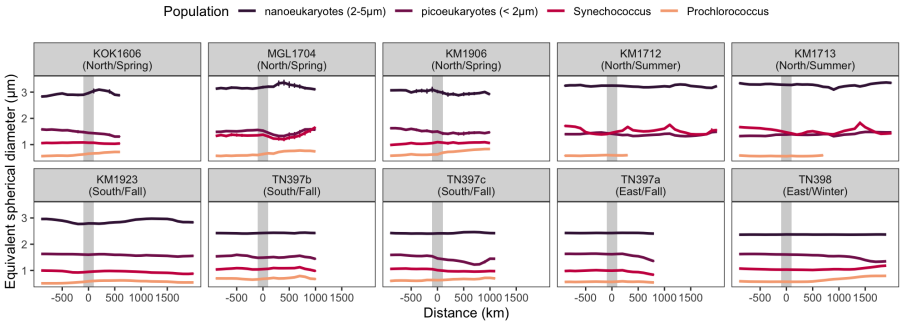

S1 Fig. Phytoplankton Cell Size Across Environmental Gradients. Phytoplankton cell size (μm ESD, equivalent spherical diameter) plotted against distance (km) from the gyre boundary (grey bar), with negative distances indicating locations within the gyre and positive distances representing locations outside the gyre. Colored lines represent the biomass of different phytoplankton groups: *Prochlorococcus* (orange), *Synechococcus* (red), picoeukaryotes (<2 μm, purple), nanoeukaryotes (2-5 μm, black). Error bars represent standard deviations of the binned data over 100 km intervals.

Acknowledgments

We thank Katherine Qi for her insights on estimating cellular growth rates from detrended carbon quota data. This work was supported by grants from the Simons Foundation (Award IDs #574495 to F.R. and #723795 to E.V.A).

References

1. Karl DM. A Sea of Change: Biogeochemical Variability in the North Pacific Subtropical Gyre. Ecosystems. 1999;2:181–214. doi:10.1007/s100219900068.
2. Chisholm SW. Phytoplankton Size. In: Primary Productivity and Biogeochemical Cycles in the Sea. Springer US; 1992. p. 213–237.
3. Acevedo-Trejos E, Brandt G, Bruggeman J, Merico A. Mechanisms shaping size structure and functional diversity of phytoplankton communities in the ocean. Sci Rep. 2015;5. doi:10.1038/srep08918.
4. Dao MH. Reassessment of the cell surface area limitation to nutrient uptake in phytoplankton. Mar Ecol Prog Ser. 2013;489:87–92. doi:10.3354/meps10434.
5. Rii YM, Karl DM, Church MJ. Temporal and vertical variability in picophytoplankton primary productivity in the North Pacific Subtropical Gyre. Mar Ecol Prog Ser. 2016;562:1–18. doi:10.3354/meps11954.
6. Worden AZ. Picoeukaryote diversity in coastal waters of the Pacific Ocean. Aquat Microb Ecol. 2006;43:165–175. doi:10.3354/ame043165.
7. Barber RT, Hiscock MR. A rising tide lifts all phytoplankton: Growth response of other phytoplankton taxa in diatom-dominated blooms. Glob Biogeochem Cycles. 2006;20. doi:10.1029/2006GB002726.

8. Taylor AG, Landry MR. Phytoplankton biomass and size structure across trophic gradients in the southern California Current and adjacent ocean ecosystems. Mar Ecol Prog Ser. 2018;592:1–17. doi:10.3354/meps12526.

9. Follett CL, Dutkiewicz S, Forget G, Cael BB, Follows MJ. Moving ecological and biogeochemical transitions across the North Pacific. Limnol Oceanogr. 2021;66:2442–2454. doi:10.1002/lno.11763.

10. Rojo C, Cobelas MA. Hypertrophic phytoplankton and the Intermediate Disturbance Hypothesis. Hydrobiologia. 1993;249:43–57. doi:10.1007/BF00008842.

11. Sommer U. An experimental test of the intermediate disturbance hypothesis using cultures of marine phytoplankton. Limnol Oceanogr. 1995;40:1271–1277. doi:10.4319/lo.1995.40.7.1271.

12. Dutkiewicz S, Follett CL, Follows MJ, Henderikx-Freitas F, Ribalet F, Gradoville MR, et al. Multiple biotic interactions establish phytoplankton community structure across environmental gradients. Limnol and Oceanogr. 2024;69(5):1086–1100. doi:10.1002/lno.12555.

13. Karl DM, Church MJ. Microbial oceanography and the Hawaii Ocean Time-series programme. Nat Rev Microbiol. 2014;12:699–713. doi:10.1038/nrmicro3333.

14. Swalwell JE, Ribalet F, Armbrust EV. SeaFlow: A novel underway flow-cytometer for continuous observations of phytoplankton in the ocean. Limnol Oceanogr: Methods. 2011;9:466–477. doi:10.4319/lom.2011.9.466.

15. Ribalet F, Berthiaume C, Hynes A, Swalwell J, Carlson M, Clayton S, et al. SeaFlow data v1, high- resolution abundance, size and biomass of small phytoplankton in the North Pacific. Sci Data. 2019;6:1–8. doi:10.1038/s41597-019-0292-2.

16. Hynes AM, Winter J, Berthiaume CT, Shimabukuro E, Cain K, White A, et al. High-frequency sampling captures variability in phytoplankton population-specific periodicity, growth, and productivity. Limnol Oceanogr. 2024; p. in press.

17. Casey JR, Björkman KM, Ferrón S, Karl DM. Size dependence of metabolism within marine picoplankton populations. Limnol Oceanogr. 2019;64(4):1819–1827. doi:10.1002/lno.11153.

18. Menden-Deuer S, Lessard EJ. Carbon to volume relationships for dinoflagellates, diatoms, and other protist plankton. Limnol Oceanogr. 2000;45:569–579. doi:10.4319/lo.2000.45.3.0569.

19. Foreman RK, Björkman KM, Carlson CA, Opalk K, Karl DM. Improved ultraviolet photo-oxidation system yields estimates for deep-sea dissolved organic nitrogen and phosphorus. Limnol and Oceanogr: Methods. 2019;17:277–291. doi:10.1002/lom3.10312.

20. Ashkezari MD, Hagen NR, Denholtz M, Neang A, Burns TC, Morales RL, et al. Simons Collaborative Marine Atlas Project (Simons CMAP): An open-source portal to share, visualize, and analyze ocean data. Limnol Oceanogr Methods. 2021;19:488–496. doi:10.1002/lom3.10439.

21. Benjamini Y, Hochberg Y. Controlling the False Discovery Rate: A Practical and Powerful Approach to Multiple Testing. J R Stat Soc Series B Stat Methodol. 1995;57:289–300. doi:10.1111/j.2517-6161.1995.tb02031.x.

22. Campbell L, Liu H, Nolla HA, Vaulot D. Annual variability of phytoplankton and bacteria in the subtropical North Pacific Ocean at Station ALOHA during the 1991–1994 ENSO event. Deep Sea Res Part I Oceanogr. 1997;44:167–192. doi:10.1016/S0967-0637(96)00102-1.

23. Karl DM, Letelier RM, Bidigare RR, Björkman KM, Church MJ, Dore JE, et al. Seasonal-to-decadal scale variability in primary production and particulate matter export at Station ALOHA. Prog Oceanogr. 2021;195. doi:10.1016/j.pocean.2021.102563.

24. Ribalet F, Swallwell J, Clayton S, Jiménez V, Sudek S, Lin Y, et al. Light-driven synchrony of Prochlorococcus growth and mortality in the subtropical Pacific gyre. Proc Natl Acad Sci USA. 2015;112:8008–8012. doi:10.1073/pnas.1424279112.

25. Martiny AC, Hagstrom GI, DeVries T, Letscher RT, Britten GL, Garcia CA, et al. Marine phytoplankton resilience may moderate oligotrophic ecosystem responses and biogeochemical feedbacks to climate change. Limnol Oceanogr. 2022;67:S378–S389. doi:10.1002/LNO.12029.

26. Carlson MCG, Ribalet F, Maidanik I, Durham BP, Hulata Y, Ferrón S, et al. Viruses affect picocyanobacterial abundance and biogeography in the North Pacific Ocean. Nat Microbiol. 2022;7:570–580. doi:10.1038/s41564-022-01088-x.

27. Johnson ZI, Zinser ER, Coe A, McNulty NP, Woodward EMS, Chisholm SW. Niche Partitioning Among Prochlorococcus Ecotypes Along Ocean-Scale Environmental Gradients. Science. 2006;311:1737–1740. doi:10.1126/science.1118052.

28. Chavez FP. Size distribution of phytoplankton in the central and eastern tropical Pacific. Glob Biogeochem Cycles. 1989;3:27–35. doi:10.1029/GB003i001p00027.

29. Frost BW, Franzen NC. Grazing and iron limitation in the control of phytoplankton stock and nutrient concentration: a chemostat analogue of the Pacific equatorial upwelling zone. Mar Ecol Prog Ser. 1992;83:291–303.

30. Blanchot J, Andre JM, Navarette C, Neveux J, Radenac MH. Picophytoplankton in the equatorial Pacific: vertical distributions in the warm pool and in the high nutrient low chlorophyll conditions. Deep Sea Res Part I Oceanogr. 2001;48:297–314. doi:10.1016/S0967-0637(00)00063-7.

31. Juranek LW, White AE, Dugenne M, Freitas FH, Dutkiewicz S, Ribalet F, et al. The Importance of the Phytoplankton "Middle Class" to Ocean Net Community Production. Global Biogeochem Cycles. 2020;34. doi:10.1029/2020GB006702.

32. Follett CL, Dutkiewicz S, Ribalet F, Zakem E, Caron D, Armbrust EV, et al. Trophic interactions with heterotrophic bacteria limit the range of Prochlorococcus. Proc Natl Acad Sci U S A. 2022;119:e2110993118. doi:10.1073/pnas.2110993118.

33. Polovina JJ, Howell EA, Kobayashi DR, Seki MP. The transition zone chlorophyll front updated: advances from a decade of research. Prog Oceanogr. 2017;150:79–85. doi:10.1016/j.pocean.2015.01.006.